Adaptive thresholds in TiO$_2$ -based synapses

Adaptive threshold in TiO₂-based synapses

N. Ghenzi[1,2,3], M. Barella[2,5], D. Rubi[1,2]and C. Acha[2,4]

[1]Gerencia de Investigaciones y Aplicaciones e Instituto de Nanociencia y Nanotecnología (CNEA); C1650B San Martín, Buenos Aires, Argentina,

[2] Consejo Nacional de Investigaciones Científicas y Técnicas (CONICET), C1033AAJ Bs. As., Argentina

[3]Facultad de Ingeniería y Agronomía, UCA, C1107AFF Bs. As., Argentina

[4]Dep. de Física, FCEyN, UBA and IFIBA-Conicet,Pab. 1,Ciudad Universitaria, C1428EHA Bs. As., Argentina

[5]Centro de Micro y Nanoelectrónica, INTI, Av. Gral. Paz 5445, B1650JKA, San Martín, Bs. As., Argentina,

corresponding author: n.ghenzi@gmail.com

Abstract: We measured and analyzed the dynamic and remnant current-voltages curves of Al/TiO₂/Au and Ni/TiO₂/Ni/Au memory devices in order to understand the conduction mechanisms and their synapse-like memory properties. Current levels and switching threshold voltages are strongly affected by the metal used for the electrode. We propose a non-trivial circuit model which captures in detail the current-voltage response of both kinds of devices. We found that, for the former device, the voltage threshold can be maintained constant, independently of the applied voltage history, while for the latter, a limiting resistor controls the threshold voltages behavior, being the origin of their dependence on the resistance value previous to the switching. The identification of the conduction mechanisms across the device allows optimizing the memristor performance and determining the best electrode choice to improve the device synapse-emulation abilities.

1. Introduction

The memristive phenomena is showing to be ubiquitous in metal - oxide interfaces [1], including some nitrides - and selenides- based devices [2, 3]. The memristor, a passive device which shows the memristive phenomena, relies on the capacity to reversibly switch between two (or more) different non-volatile resistance states. These devices were initially proposed to be used in the next generation of non-volatile memories [4-5], though in the last years logical computing and synaptic emulation capabilities for neuromorphic computing were found [6-9].

Although multilevel operations in the memristor can be technologically exploited, the physical mechanisms and their control remain elusive. In many cases, the modulation of the barrier at the metal- oxide interface due to the movement of oxygen vacancies explains the switching between different resistance states [10]. In these cases, resistive switching needs oxygen vacancies to overcome the potential barrier existing between different lattice sites. This barrier is surpassed through an applied voltage generating an electric field in the order of 10^{7-8} V/cm. An important key of technological relevance is to understand exactly which parameters control the switching threshold as well as its underlying mechanisms. In the vast majority of papers [1-18 and references there in] the modulation of the Schottky barrier (SB), present at oxide-metal interfaces, due to the electromigration of oxygen vacancies was proposed as the active memristive mechanism.. On the other side, the conduction properties inside the oxide could play an active role in the RS. One of the possible conduction mechanisms between metallic electrodes and dielectric oxides is the space charge limited current mechanism (SCLC) [19-22]. The SCLC conduction is related to the excess injection of carriers from the electrode to the dielectric material and their spatial accumulation effects, leading to different conducting regimes, depending on the degree of disorder of the oxide [23]. The Child regime is characterized by a quadratic current–voltage dependence ($I\sim V^2$) [24-27].

The memristor ability to mimic the long term potentiation plasticity of the synapse has been studied during the last ten years [6], showing that memristors can reproduce spike timing dependent plasticity (STDP) with low energy consumption. The STDP biological process is one of the fundamental mechanisms for learning and making memories in the brain. This turns memristors as suitable devices for the development of artificial synapses, beyond standard silicon-based electronics [7]. Generally, the STDP rule is realized in memristors with a fixed voltage threshold determining the weight synaptic modification [8]. Nevertheless, variable thresholds are also used and observed in biological synapses, what makes them a very promising aspect for constructing memristive neural networks as shown in ref. [28].

Classical learning algorithms for neural networks are characterized by a learning rule which computes synaptic weight changes by multiplication of three variables: two variables related to the pre- and post-synaptic activity and an additional reinforcing feedback variable. In a biological context, the reinforcing feedback variable can be interpreted as a rewarding or punishing signal emitted by the animal´s environment [28]. The rewarding or punishing of the sensory cue in the input of the neural network can be emulated with Hebbian synapses with adaptive thresholds [29].

Here we show that the switching voltage threshold of the resistive switching (RS) effect on metal-TiO₂ (amorphous)-metal devices (metal= Al, Au and Ni) strongly depends on the electrode metals. For each combination of electrodes, by analyzing the I-V characteristics, we determined the equivalent electric circuits, indicating in all cases a complex scenario.

The equivalent circuit, for both devices, includes a leaky Schottky Barrier (SB) associated with the metal-TiO$_2$ interface, SCLC conduction through TiO$_2$ and an ohmic channel probably associated with Magneli-like phases. The main difference between the explored devices is the existence (or absence) of a relevant series resistance that limits both the Schottky conduction and the ohmic channel (present only for the Ni devices) and modifies the behavior of the switching voltage threshold between fixed or adaptive behavior. Commonly, researchers who study memristors deal with fixed voltage threshold devices rather than memristors with dynamic threshold. In this work, we show memristive devices with externally controllable voltage threshold, a kind of device that is missing in literature and needs to be developed in order to have artificial synapses with adaptive thresholds [28].

2. Methods

We fabricated TiO$_2$ vertical junctions of 100 μm x 25 μm area in a crossbar pattern (Fig.1). TiO$_2$ films were deposited by reactive sputtering with a pressure of 20 mTorr, and a power of 150 W at room temperature. We should remark that the combination of ellipsometry, XPS and microscopy data suggests that our films microstructure is compatible with a network of poorly crystallized nanograins.
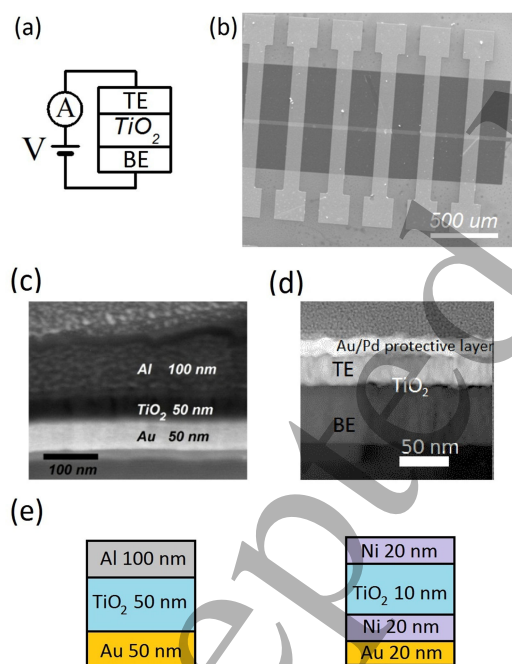
Fig. 1: (a) Schematic of the electrical connections. Voltage is applied to the top electrode. (b) General view of the devices showing their crossbar structure. Typical cross section SEM images of the (c) Al/TiO$_2$/Au and (d) Ni/TiO$_2$/Ni/Au devices. (e) Schematic of the fabricated devices.

The metals acting as bottom (BE) and top (TE) electrodes were deposited by DC sputtering in an argon atmosphere with thicknesses between 20 and 100 nm, depending of the electrode. To get the crossbar pattern we employ a lift off process to define each one of the three layers of the junction (BE= Au and Ni, TiO$_2$ and TE= Al and Ni) [15]. The TiO$_2$ film thickness was 50 nm for the Al/TiO$_2$/Au device (Fig. 1(c) and it was 10 nm for the other device (Fig. 1(d)). We chose the Au electrode to provide a SB in the first device. In the other device we used Ni, which is an oxidizable electrode and may allow the appearance of defects at the interface, giving place to a less conducting device. The electrical characterization (*I-V* curves) was performed with a source-measurement unit Keithley 2612B, with the BE grounded. Fig. 1(e) shows a schematic of the fabricated devices.

3. Results and discussion

We study the *I-V* response of the two devices. Our results are shown in Fig. 2. For the case of the Al/TiO$_2$/Au device it was necessary to apply a forming process with a 1 mA current compliance (bottom inset of Fig. 2(a)) while the Ni/TiO$_2$/Ni/Au devices respond as a forming free device. In the top inset of Fig. 2(a) we show the Ni/TiO$_2$/Ni/Au typical response in linear scale. Measurements on the Al/TiO$_2$/Au device are qualitatively similar (Fig. 2(a)), in spite of quantitative differences in both current and voltage ranges. The electrical response for both devices presents two highly non-linear resistance states with gradual SET and RESET transitions in opposite polarities, indicating the existence of bipolar resistive switching. In Fig. 2(b) we show the corresponding I-V responses in a Log-Log plot.

The two I-V curves show hysteresis with two stable resistance states corresponding to the high resistance HR and low resistance LR states. The SET transition (HR to LR) occurs in positive voltage while the RESET transition (LR to HR) occurs in negative voltage for both devices. The SET voltages are +1V and +3V while the RESET voltages are -1.3 V and -3.7 V for the Al/TiO$_2$/Au and Ni/TiO$_2$/Ni/Au devices, respectively. The required compliance current values to induce a reproducible resistive switching were fixed at 5 mA and 1 mA, respectively. Both I-V responses show non-linear HR and LR states in the explored voltage ranges, as usually found in bipolar RS devices [10].

Bipolar RS is related to oxygen vacancies movement from/to the metal oxide interface and the bulk of the oxide, where non-percolating conductive filaments are formed during the first I-V cycles (or during the electroforming) [10]. Due to the polarity of the SET and RESET transitions the conductive filaments are fully connected to the TE, becoming in a reservoir of oxygen vacancies. This indicates that the active interface (where the OVs move) for the switching is the bottom electrode-oxide one, having a

higher resistivity than the top electrode-oxide interface. Then the Au and Ni metals are the active electrodes originating the resistive switching effect in each one of the corresponding devices.
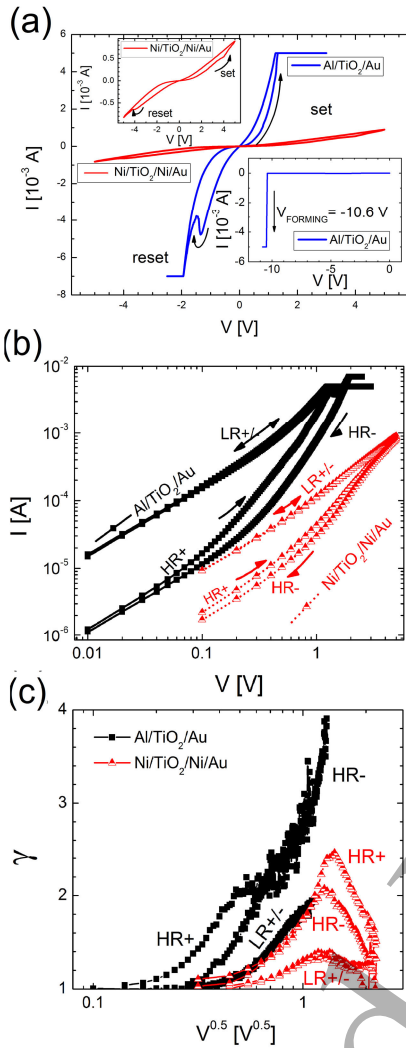
***Fig. 2**: (a) Typical I-V response of Al/TiO₂/Au junction. Bottom inset : corresponding electroforming process. Top Inset : Typical I-V response of the forming-free Ni/TiO₂/Ni/Au junctions. (b) Log(I)-Log(V) response for the two types of sample. c) Logarithmic derivative $\gamma = d(LnI)/d(LnV)$ as a function of $V^{0.5}$ for the two samples in the HR +/- and LR+/- states. The obtained gamma curves indicate clear differences between devices: The Al/TiO₂/Au device shows two non-linear conduction processes while the Ni/TiO₂/Ni device shows additionally an ohmic serie conduction which limits and dominates the conduction for voltages higher than 1 V.*

At a first glance, the I-V characteristics shown in Fig. 2(b) seem similar for both devices. It is also difficult to determine a single conduction mechanism as, depending on the voltage range, different power laws can be envisioned. It has already been shown the usefulness of a graphical method based on the power exponent parameter [$\gamma = d(LnI)/d(LnV)$] in order to

reveal the main conduction mechanisms through a device [22]. For example, when γ is plotted as a function of $V^{1/2}$ a Schottky emission is represented by a straight line passing through the origin. Nevertheless the power of this method becomes clearly evident when more than one conduction mechanism is present, as it is usually the case of memristors based on complex oxides [22-24].

As can be observed in Fig. 2(c), our results show complex γ vs. $V^{1/2}$ curves. Although all the devices show a γ close to 1 (ohmic) for low voltages, clear differences can be observed between the Al/TiO₂/Au device with respect to the other (Ni/TiO₂/Ni/Au). Indeed, for the former device, the HR states for both polarities show a monotonic increase of γ up to values close to 4 with a small plateau around ~ 2. While for the other device, the γ response for both polarities in the HR and LR states show much lower values (γ<2.6) and a positive skewed distribution shape with respect to $V^{0.5}$. The switching to a more conducting device (LR) it is also associated with a more ohmic dependence (lower γ values), although the non-linear elements are still present.

This particular shape of the γ parameter for Al/TiO₂/Au indicates the existence of at least two non-linear mechanisms with the presence of a parallel ohmic leak, while for Ni/TiO₂/Ni/Au the non-linear conduction is limited by ohmic elements in series. This qualitative behavior is going to be the basis for the proposal of the basic elements that build the equivalent circuit model, as will be discussed later.

We have also explored the non-volatile response of the two devices by measuring their hysteresis switching loops (HSL) in order to determine the resistance levels and voltage thresholds (Fig. 3). We chose to stimulate the devices with voltage in a pulsed loop mode with write and read pulses. Writing voltage pulses of 10 ms time width and variable amplitude between +/- V_{MAX} were followed by a small constant read pulse of 0.1 V amplitude and 250 ms of time width. In the inset of Fig. 3(a) is shown the pulsing protocol. We named the protocol of pulsing between +V_{MAX} and -V_{MAX} as "major loops". Fig. 3 shows the current read at 0.1 V (proportional to the conductance of the device) as a function of the amplitude of the writing pulse for the (a) Al/TiO₂/Au and (b) Ni/TiO₂/Ni/Au devices. In both cases we obtain HR and LR states with the SET transition in positive voltage and the RESET transition in negative voltage, as we mention before.

With the purpose of showing the characteristics of the intermediate states, after doing one major loop, we stopped the pulsing protocol when applying negative pulses, i.e. in the middle of the RESET transition. Instead of continuing increasing the amplitude of negative pulses, we began to decrease the amplitude of the negative voltage. We swept the amplitude till the maximum positive voltage and we returned to the

initial negative voltage. We named this protocol as "minor loops". In both types of devices we obtained multi-level resistance states with the same characteristics than the extreme resistance ones.
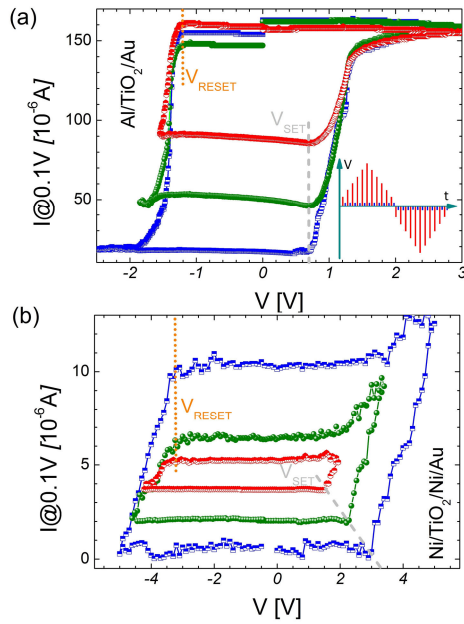
Fig.3: *Hysteresis switching loops (HSL) response for the samples of (a) Au/TiO₂/Al and (b) Ni/TiO₂/Ni/Au. In (a) we obtained independent threshold voltages of the resistance states, while in (b) the SET voltages depend on the initial resistance states.*

We now turn to describe in detail the results in the Al/TiO₂/Au devices of Fig. 3(a). As observed in the major loop, the non-volatile current (@0.1 V) exhibits two well-defined states around 170 and 20 µA (600 Ω and 5kΩ). The switching produces a factor of almost 10 between the maximum and minimum read current. The SET and RESET threshold voltages are in +1 V and -1.3 V respectively. In the case of the minor loops, e.g. in that corresponding to a minimum voltage of -1.5 V, we obtained a read current of 70 µA (1.4 kΩ), a value between the maximum and minimum read current of 170 and 20 µA. We repeat the process of minor loops obtaining 3 different resistance states. The most noticeable feature is that the threshold voltages for switching the device are independent of the resistance state, being 1 V for the SET transition and -1.3 V for the RESET transition for all measured loops.

For the Ni/TiO₂/Ni/Au devices, the extreme states are around a non-volatile current (@0.1 V) of 0.5 and 10 µA, with a SET transition in 3V and a RESET transition in -3.5 V. We measured 2 minor loops with the non-volatile current values between the two extreme values. In this case, the RESET voltage is independent of the resistance states (orange dotted line). Nevertheless, the SET threshold voltage

strongly depends of the resistance state (gray dashed line). This behavior is similar to the adaptive threshold mechanism of biological synapses. In the neural network context, the adaptive threshold can favor (reward) synaptic connection when the voltage threshold for the resistive switching is decreased due to a low resistance value of the corresponding synapse [30]. On the other side, when the synaptic connection is not so strong (high resistance value), a punishment is produced increasing the voltage threshold for the resistive switching. It is widely known that different synapses differ in their ability to regulate or influence the activation of a biochemical mechanism (Ca^{2+} concentration) for synaptic weight changes [30]. How the thresholds are modified by the previous history of reinforcing feedback resembles the change in the dynamics of Ca^{2+} signals and is not reproduced by classical STDP implementations, being needed an adaptive threshold behavior as the one shown by our Ni/TiO₂/Ni/Au devices.

We go back now to the γ-analysis. The complex evolution of this parameter (Fig. 2) can be ascribed to the existence of two non-linear conduction mechanism in parallel, that require an ohmic leak (γ ≈ 1), also in parallel, to account for the low V behavior. The increase of γ from 1 to the plateau value when increasing V indicates the crossover from ohmic conduction at low V to SCLC conduction (Child's law) at intermediate V. In the case of the Al/TiO₂/Au device, the further increase in the value of γ for the highest voltages indicates a conduction dominated by Schottky emission, which for the Ni devices is limited by a series ohmic resistance [31]. It is interesting to note that, for all the junctions, the shape of γ is quite similar for both polarities, indicating a symmetric distribution of circuit elements, independently of the metals used for both electrodes.

This complex scenario was simulated by proposing 6 different equivalent circuits (including more symmetric configurations and also Poole-Frenkel non-linear elements) and by solving numerically their transcendental and implicit I-V equations [23]. The best fits (see Fig. 4 and Fig. 5) were obtained by considering the circuit model shown in Fig. 4(a) for both devices, described by the following equations:

$$I = I_{Scht,b} + I_{SCLC} + I_R ,$$

with

$$I_{Sch} = I_{Satt,b} \left[e^{(a_{t,b}\sqrt{V-I_{Sch}R_{t,b}})} - 1 \right],$$

$$I_{SCLC} = AV^N ,$$

$$I_R = \frac{I}{R},$$

and $a_{t,b} = \frac{q^{3/2}}{k_B T\sqrt{4\pi\varepsilon' d}}$,

4

Where $I_{Scht,b}$ is the current through the top or the bottom Schottky diode (relevant for the positive or negative polarity, respectively), I_{Sat} its saturation current, I_{SCLC} and I_R the current through the SCLC and the ohmic channel, respectively, q is the electron's charge, ε' the real part of the dielectric constant of the oxide and d, a relevant width where most of the voltage drops.
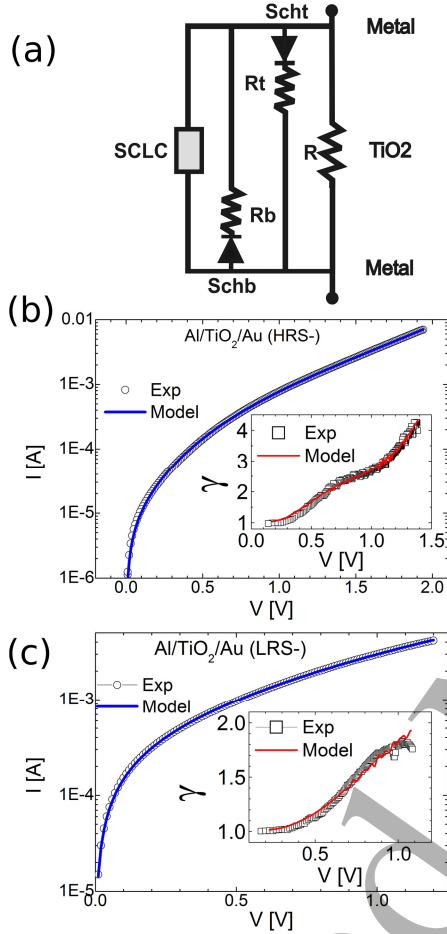
Fig 4: (a) Equivalent circuit model proposed for both devices (Al/TiO₂/Au and Ni/TiO₂/Ni/Au). (b) Experimental and simulated I-V response in the HR-state for the Al/TiO₂/Au devices. Inset: corresponding experimental and simulated γ representation. (c) I-V response in the LR- state for the Al/TiO₂/Au devices. Inset: corresponding γ representation. (Similar results were obtained for HR+ and LR+).

In Fig. 4 and Fig. 5 we show the excellent fits obtained for the Al/TiO₂/Au and the Ni/TiO₂/Ni/Au junctions, respectively, not only of the I-V characteristics but also of the more exigent γ representation. The proposed equivalent circuit reveals the degree of non-ideality of our devices, although this seems to be a standard feature of metal-oxide junctions [22-24 and references therein]. It should be considered that the voltage-enhanced oxygen mobility [33], the competition between the oxidation energy of metals and oxides [34], as well as the electroforming process [35] may produce a highly

inhomogeneous distribution of oxygen along the device. This introduces electrical carrier traps in the TiO₂ insulating matrix as well as conducting defects which may lead to the formation of localized conductive channels or, if localized at the interface, to modifications of the expected Schottky barrier [36].
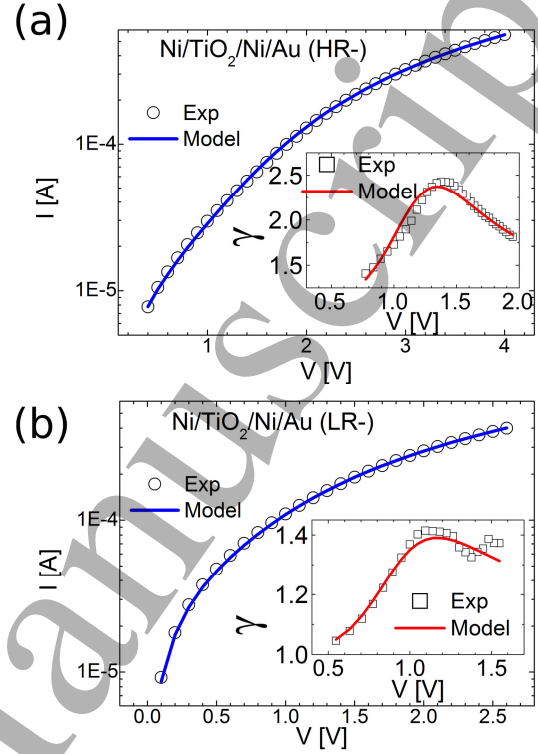
Fig. 5: Modeling the I-V response of Ni/TiO₂/Ni/Au devices. (a) Experimental and simulated I-V response in the HR- state. Inset: corresponding experimental and simulated γ representation. (b) I-V response in the LR- state. Inset: corresponding γ representation. (Similar results were obtained for HR+ and LR+).

Within this framework, our results indicate the existence of three parallel conducting channels for each polarity: a Schottky emission at both interfaces, a SCLC through the oxide as well as an ohmic resistor, probably provided by Magnéli-like phases [37]. These parallel channels are probably interconnected with a highly resistive TiO₂ interface but, due to the conductivity difference with the non-stochiometric phases, the TiO₂ contribution can be disregarded.

The fact that switching from HR to LR states is produced when applying a positive voltage to the top electrode is in accordance to the expected migration of oxygen-vacancies from top (conductive filament acting as OV reservoir) to bottom (active interface). As previously mentioned, the creation of oxygen-vacancies in TiO₂ may produce charged defects when isolated and conducting channels when grouped. This asymmetric-voltage creation of the conducting channel can be related to the fact that oxygen ions

would drift-diffuse easier when moving out of the top electrode than through the bottom one, due to the barrier imposed by the substrate [21].

Fitted parameters associated with each element of the circuit model presented in Fig. 4(a) are summarized in Table I for both HR and LR states.

Parameter	HRS Al-TiO$_2$-Au	LRS Al-TiO$_2$-Au	HRS Ni-TiO$_2$-Ni-Au	LRS Ni-TiO$_2$-Ni-Au
a_t [V$^{-1/2}$]	6.9	5.8	3.8	9.0
I_{satt} [A]	10^{-6}	10^{-6}	$6 \cdot 10^{-7}$	$6 \cdot 10^{-9}$
R_t [kΩ]	0	0	0	7.4
a_b [V$^{-1/2}$]	8.8	3.1	7.4	7.1
I_{Satb} [nA]	18	18	6	10
R_b [kΩ]	0	0	3.9	3.5
A [A/V^N]	0.006	0.0016	$3 \cdot 10^{-6}$	0
N	2.64	2.59	2	2
R [kΩ]	11.4	0.7	60	12

Table I: *Fitted parameters of the circuil model of Fig. 4(a) associated with the Al/TiO$_2$/Au and Ni/TiO$_2$/Ni/Au devices. Blue and red cells indicate an oxygen or a vacancy rich TiO$_2$, respectively.*

The main difference between the Al/TiO$_2$/Au and the other device is esentially related to the series resistors R_b and R_t. For the former device these resistances can be neglected. The forming process in this device may have introduced more conducting channels than in the other, so the overall resistance of the device is lower.

By analyzing the results of the equivalent circuit together with the threshold behavior when stimulating with major and minor loops, the main effect produced during a SET transition for the Al/TiO$_2$/Au device, is to increase the conductivity of the ohmic channel. As V_{SET} and V_{RESET} are independent of the resistance state, we can infer that pulses drift OV´s, creating or destroying an increasing number of conducting filaments within a fixed distance d.

On the other side, in the Ni/TiO$_2$/Ni devices, the switching from LR to HR (by applying negative pulses) produces additional changes in the series resistors as well as on the top Schottky diode: R_b increases while R_t strongly decreases and the inverse saturation current of the diode increases probably as a decrease in the SB. This suggests that during the RESET oxygen vacancies migration from the bottom to the top of the device occurs, thus generating a difference in conductivities between the regions near each electrode, resulting in a voltage-divider circuit. In this way, the device becomes more insulating by driving oxygen to the TiO$_2$ bulk while vacancies are located near the top interface.

The presence of positively charged defects (oxygen vacancies) in the top interface may reduce the SB as was observed in the case of hydrogen absorption in the Pt/TiO$_2$ interface [22]. As far as the device becomes more insulating by extending the application of negative pulses (see the turning points of the HSL shown in Fig. 3), the electric field strength at the top electrode interface is further reduced determining the need to increase the positive threshold voltage (V_{SET}) to force the SET transition. Finally, as an increasing number of percolating filaments are established between the electrodes during the SET process, V_{RESET} becomes history-independent, as in the case of the Al/TiO$_2$/Au device.

In Fig. 6 we show the long term potentiation (LTP) and depression (LTD) properties of both devices. 50 pulses of +/- 2V were applied for potentiation and for depression processes.
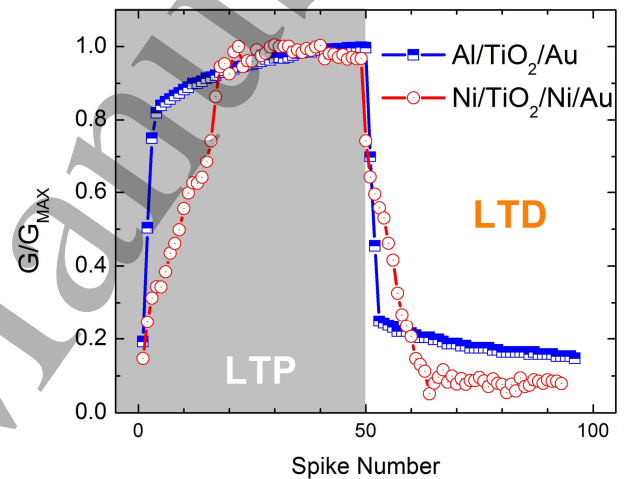
Fig. 6: *Long term potentiation and depression responses of the Al/TiO$_2$/Au and the Ni/TiO$_2$/Ni/Au devices.*

The conductance response in both devices exhibits an increase with positive pulses and a decrease for negative pulses, concomitant with the oxygen vacancies movement in the bottom interface. In the Al/TiO$_2$/Au we observe an exponential behavior of the conductance as a function of the number of spikes, while in the Ni/TiO$_2$/Ni/Au we observe a linear behavior with saturation after 15 spikes. In ref. [38] recognition rate of handwritten numbers is studied for a three layer neural network with unsupervised learning, for different non- linear modulation coefficients of the LTP and LTD properties. Although the non-linearity of the LTP and LTD properties is not critical in maintaining the recognition rate; the recognition rate is reduced in 6% from the linear to the exponential case. This indicates that our Ni/TiO$_2$/Ni/Au devices would likely show a better behavior in a neural network as compared to the Al/TiO$_2$/Au one.

4. Conclusions

In summary, the resistive switching behavior of metal/TiO$_2$/metal devices with different combinations of metal electrodes (Al-Au and Ni-Ni/Au) was investigated. We have measured the I-V characteristics, the non-volatile hysteretic response HSL and LTD and LTP curves. We observed that the switching voltage threshold follows two different behaviors depending on the metallic electrode of the device, *i.e*, fixed or adaptive thresholds. This behavior can be used to reproduce biological synapses with adaptive thresholds to implement in artificial neural networks. In order to disclose the reasons of the different I-V and HSL responses, we proposed a circuit model for each device which captures the detailed I-V dependence. The circuit model reveals the complexity of the electrical conduction scenario. The coexistence of the proposed parallel and series elements evidence the presence of inhomogeneous junctions that give different conduction mechanisms as a consequence of the disorder introduced by voltage-assisted oxygen migration, as well as by the oxidation energy competition of the involved metals. Although the presence of SB contributions and SCLC conduction should be considered, the main effects produced by switching are related to changes in the conductivity of the ohmic channel. The differences on the switching voltage behavior can then be ascribed to the existence (or not) of an interfacial resistor that acts as a voltage divider, which modify the local electric field and concomitantly, the threshold voltage needed to produce the resistance change of the device.This basic approach of circuital modeling with a systematic study of the electrical behavior can guide the optimization of memristor devices for novel electronic applications.

References

[1] D. Ielmini and H. S. Wong, Nature Electronics **1**, 333 (2018).

[2] D. Kumar *et al*, Appl. Phys. Lett. **110**, 203102 (2017).

[3] I. Roppolo *et al*, J. Phys. Chem. C **121**, 14285 (2017).

[4] L.Chua, IEEE Transactions on circuit theory **18**, 507 (1971)**.**

[5] T. D. Dongale *et al*, Journal of Nanoscience and Nanotechnology **18** (11), 7758 (2018).

[6] T. D. Dongale *et al*, Journal of Nanoelectronics and Optoelectronics **13**, 68 (2018).

[7] Dmitri B. Strukov *et al*, Nature **453**, 80 (2008).

[8] D. S. Jeong, H. Schroeder, and R. Waser, Phys. Rev. B **79**, 195317 (2009).

[9] K. Yoon *et al*, Nanotechnology **23**, 18 (2012).

[10] J. J. Yang *et al*, MRS Bull. **37**, 131 (2012).

[11] D. Ielmini, Microelectronic Engineering **190**, 44 (2018).

[12] S. H. Jo *et al*, Nano. Lett. **10**, 1297 (2010).

[13] C. Wu *et al*, Nat. Comm. **8**, 752 (2017).

[14] C. Z. Ramos *et al*, Front. Neurosci.**5**, 26 (2011).

[15] W. Cai, F. Ellinger and R. Tetzlaff, IEEE trans. on biomedical circuits and systems 9, 87 (2015).

[16] N. Ghenzi *et al*, Appl. Phys. Lett. **104**, 183505(2014).

[17] S. Wang *et al*, Nanoscale Res. Lett. **13**, 18 (2018).

[18] A. Kindsmuller, APL Materials **6**, 046106 (2018).

[19] C. Acha, J. Appl. Phys. **121**, 134502 (2017).

[20] F. Chiu, Adv. In Mat.Sc.and Eng. Vol 2014, Article ID 578168 (2014).

[21] N. Ghenzi *et al*, Appl. Phys. Lett.**106**, 123509 (2015).

[22] C. Acha, Journal of Physics D: Applied Physics **44**, 345301 (2011).

[23] C. Acha, A. Schulman, M. Boudard, K. Daoudi and T. Tsuchiya, Appl. Phys. Lett. **109**, 11603 (2016).

[24] W. R. Acevedo, C. Acha, M. J. Sánchez, P. Levy and D. Rubi, Appl. Phys. Lett. **110**, 053501 (2017).

[25] C. Yoshidaa, K. Tsunoda, H. Noshiro and Y. Sugiyama, Appl. Phys. Lett. **91**, 223510 (2007)

[26] H. Schroeder and D. S. Jeong, Microelectronics engineering **84**, 1982 (2007).

[27] H. Zhang et al, ACS Appl. Mater. Interfaces **10**, 29766 (2018).

[28] Pennartz C.M.A, Neuroscience **81**, 303 (1997)].

[29] W. Cai and R. Tetzlaff, "Advanced memristive model of synapses with adaptive thresholds" **13**th International workshop on cellular nanoscale networks and their applications, pp 1-6. (2012).

[30] D Bolle and R. Heylen, International Journal of Neural Systems **17**, 241 (2007)

[31] D. Sahu and S. Jammalamadaka, Scientific Reports **7**, 17224 (2017).

[32] D. H. Kwon *et al*, Nature Nanotechnology **5**, 148 (2010).

[33] A. Sawa, Mater. Today **11**, 28 (2008).

[34] S. H Jeon and B.H. Park, Appl. Phys.Lett**89**, 042904 (2006).

[35] R. Ciencia *et al*, Phys. Rev. B **86**, 104110 (2012).

[36] F.G. Marlasca *et al*, Appl. Phys.Lett **98**, 123502 (2011).

[37] D. Cerchez *et al*, Appl. Phys. Lett **103**, 033522 (2013).

[38] S. Kim, M. Lim, Y. Kim, H. D. Kim and S. J. Choi, Scientific Reports **8**, 2638 (2018)